Reply to Referee #1:

The article focuses on studying the interactions between hydrological processes involving karst aquifers, conduits, and streams, varying with precipitation and other factors that are later described in detail. The work is well-structured, the figures are of good quality, and the reading is fairly smooth.

Dear Reviewer: Thank you very much for your comments and suggestions. Our replies are listed as follow:

(1) The topic is, in my opinion, significant but somewhat self-contained when the discussion remains limited to numerical results without extending them to a broader analysis—namely, how this study could be useful in managing water resources in these complex aquifers or how it could be applied at a regional scale.

Thank you for pointing out the need to strengthen the practical application relevance in the Discussion section. In response to this suggestion, we have added implications of modeling parameters for karst water resources management in the revised version, as follows:

- Lines 725-730: Discusses the effect of conduit geometry (e.g., square cross-section) on aquifer-stream interaction fluxes, emphasizing its critical role in enhancing simulation accuracy.
- Lines 756-763: Analyzes the regulatory mechanism of epikarst permeability on groundwater flow paths, illustrating the importance of parameter calibration for water resources prediction.
- Lines 781-792: Adds an analysis of the impact of porosity parameters on karst water resources allocation and geological stability, clarifying the model's potential application in flood warning.

Lines 725-730:

"Conduit geometry (radius and shape) constitutes a critical factor in karst aquifer hydrological modeling. Larger circular conduits accelerate peak discharge arrival and amplify stream-connected flow peaks and karst spring discharge. Square-section conduits outperform circular equivalents in peak discharge capacity under identical nominal radii due to cross-sectional area advantages. Enlarged conduits intensify porous medium-stream interactions and amplify PM III recharge through gravitational effects. Comprehensive consideration of conduit geometry impacts on hydrological elements is essential for improving model accuracy and reliability in simulating karst aquifer-stream interaction processes."

Lines 756-763:

"Epikarst permeability constitutes a critical factor in hydrological modeling of karst aquifer systems. Highly permeable epikarst produces rapid streamflow peaks followed by sharp declines, reflecting efficient groundwater leakage to the stream. Conversely, low permeability yields diminished peaks and broader discharge curves. While karst spring discharge remains relatively stable when epikarst permeability differs from porous media, proper characterization of epikarst permeability is essential for accurately simulating hydraulic interactions between media, regulating groundwater flow pathways and velocities. This enhances model reliability in capturing complex flow dynamics within karst conduit-stream systems."

Lines 781-792:

"In hydrological modeling, porosity parameters must be calibrated to accurately simulate groundwater flow paths and storage-release dynamics. For low-porosity regions, models should emphasize rapid drainage capacity of conduit systems and transient flow variations. In high-porosity areas, considerations should include fluid retention risks, stream-porous media interactions, and their long-term impacts on geological stability and water resource allocation. Proper porosity parameterization enhances simulation accuracy for diverse hydrological processes, enabling improved prediction and management of karst water resources.

Karst hydrological vulnerability manifests prominently through rapid infiltration, epikarst runoff, groundwater table fluctuations, and abrupt spring discharge variations. The DBS model effectively simulates multi-media interactions during extreme recharge events, enabling temporal analysis of media-stream exchanges, identification of peak interaction values, and applications in coupled conduit flow-seepage processes for two-phase flow systems."

(2) The analytical and numerical approach is based on a representative sample of an aquifer, with the conduit size set by the authors (which I also find quite large) and a variation in rainfall intensity that I do not understand, as it is measured in meters according to Table 1. In hydrology, rainfall intensity is measured in mm/h, representing the amount of rainfall per unit of time. I kindly ask the authors to better define this aspect and, if necessary, correct it.

Thank you for your corrections regarding the units for conduit dimensions and precipitation intensity:

- Rationality of conduit dimensions: We have added a parameter sensitivity analysis (Lines 698-731), which quantifies the impact of different conduit diameters (0.2–0.5 m) and cross-sectional shapes (circular/square) on fluxes between media components using Fig. 12. This validates the physical basis for the parameter settings.
- Correction of precipitation intensity unit: The entry "Precipitation intensity (m)" in Table 1 was a typographical error; we have deleted this column. Furthermore, detailed definitions of the precipitation function have been added in the "2.5 Rainfall Infiltration Recharge

Boundary" subsection (Lines 345-353614-633): The precipitation function is defined as a time-dependent variable I(t), with its intensity modulated by the dimensionless parameter b, consistent with conventional expressions in the hydrology field.

Lines 698-731:

"4.1 Impacts of Conduit Diameter and Geometry on Interactions Between Karst Aquifer Systems and Streams

Fig. 12 presents hydrographs under conditions of circular conduits with varying radii (r=0.2, 0.3, 0.3, and 0.5 m) and square-section conduits (r=0.5 m) for (a) stream-connected flow, (b) karst spring discharge, (c) epikarst flow, (d) porous medium I (PM I), (e) PM II, and (f) PM III. Fig. 12(c.1) illustrates different conduit cross-sectional shapes to analyze their impacts on the interactive flow between karst aquifer systems and adjacent streams.

As shown in Fig. 12(a), larger conduit radii correspond to higher initial discharge peaks and shorter peak arrival times, indicating enhanced porous medium recharge and faster fluid transmission through larger conduits. Notably, the square-section conduit (s-r_c=0.5) exhibits higher peak discharge than its circular counterpart (rc=0.5) due to its surplus cross-sectional area accommodating greater fluid discharge under identical nominal radii.

Fig. 12(b) demonstrates that karst spring peak discharge increases with conduit radius. At r=0.5 m, the square-section conduit ($s-r_c=0.5$) achieves higher peak discharge than the circular conduit ($r_c=0.5$), but displays lower recession flow. This occurs because identical precipitation infiltration recharge leads to greater porous medium storage depletion during peak periods in square conduits, subsequently reducing porous medium-to-conduit recharge during baseflow recession.

Combined analysis of Figs. 12(c), (d), and (e) reveals that conduit radius variations do not significantly affect epikarst hydrographs or PM I/II hydrographs. However, square-section sinkholes modify flow patterns: epikarst hydrographs show lower values under square conduits, while PM I/II hydrographs exhibit higher values due to enhanced epikarst groundwater collection in square cross-sections, increasing recharge to PM I/II.

Fig. 12(e) indicates that larger conduit radii correspond to lower negative values. Combined with Fig. 12(a), this demonstrates that increased stream recharge through larger conduits elevates both stream peak discharge and water levels, thereby enhancing porous medium-stream interactions. Similarly, Fig. 12(f) shows that larger conduit radii increase karst spring discharge and PM III hydrograph elevation through enhanced gravity-driven groundwater recharge.

Conduit geometry (radius and shape) constitutes a critical factor in karst aquifer hydrological modeling. Larger circular conduits accelerate peak discharge arrival and amplify stream-connected flow peaks and karst spring discharge. Square-section conduits outperform circular equivalents in peak discharge capacity under identical nominal radii due to cross-sectional area advantages. Enlarged conduits intensify porous medium-stream interactions and amplify PM III recharge

through gravitational effects. Comprehensive consideration of conduit geometry impacts on hydrological elements is essential for improving model accuracy and reliability in simulating karst aquifer-stream interaction processes."

Lines 1084-1088:

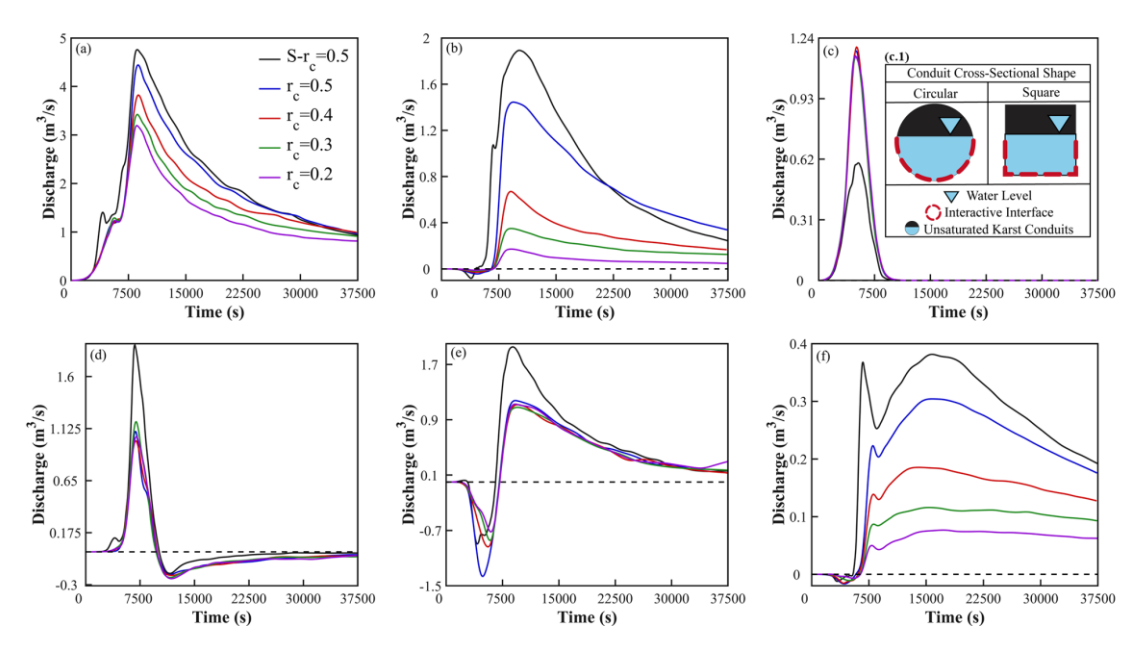


Figure 12. Hydrological process curves for (a) stream, (b) karst spring, (c) epikarst, (d) PM I, (e) PM II, and (f) PM III under conditions of circular conduits with radii $r_c = 0.2, 0.3, 0.3,$ and 0.5, and square-cross-section conduits with S-r_c = 0.5. Subplot (c.1) shows a schematic diagram of different conduit cross-sectional shapes.

Lines 345-353:

"2.5 Rainfall Infiltration Recharge Boundary

The upper boundaries of both the DBS and CFPv2 models are defined as transient natural precipitation boundary conditions. In this study, the rainfall infiltration recharge boundary condition is formulated as follows (Huang et al., 2024; Chang et al., 2015):

$$I(t) = \frac{b}{\sqrt{2\pi\sigma^2}} \sum_{i} e^{-\frac{\left(\frac{t_i - \mu}{a}\right)^2}{2\sigma^2}} \tag{1}$$

Here, t_i denotes the time of the *i*-th rainfall event, and I(t) represents the total rainfall amount at that time. According to Chang et al. (2015), the parameters $\mu \setminus \sigma^2$, and a are set as constants (90, 1.5, and 20, respectively). Variations in rainfall intensity during the infiltration recharge process are controlled by adjusting the value of the dimensionless parameter b."

- (3) Another aspect concerns the discussion section. This should compare the obtained results with those in the literature, discuss the limitations and advantages of such an approach, perform a sensitivity analysis on the calibrated parameters, and assess the study's usefulness and general applicability. The current section focuses on comparing the results with those from the MODFLOW-CFP model, which the authors themselves implemented. In my opinion, this should still be described in the results section, and consequently, the methodological section should be expanded to include this additional approach.
 - Acknowledgments for your suggestions regarding results comparison and chapter organization:
 - Literature comparison: Added quantitative validation against experimental data from Warrick et al. (1985) and Vauclin et al. (1979) (Lines 614-633), demonstrating the reliability of the DBS model in simulating variably saturated flow.
 - Chapter restructuring: Relocated the MODFLOW-CFPv2 comparison section to the "Results" chapter (Lines 301-303) and expanded the explanation of CFPv2 principles in the "Methodology" section (Lines 281-291).

Lines 614-633:

"The external recharge of the system significantly influences the interaction processes among different media. This study further investigates how the inherent hydrogeological properties of karst systems affect these interactive processes. Variable saturated flow in the karst vadose zone plays a critical role (Dvory et al., 2018), where the water retention characteristics of porous media govern unsaturated flow dynamics. However, the CFPv2 model struggles to simulate variable saturation processes. This paper compares the DBS model results with two distinct experimental datasets to elucidate the advantages and limitations of the DBS approach in simulating variable saturated flow.

Case 1: A typical unsaturated-unsteady seepage problem in sandy clay loam (Warrick et al., 1985), where the soil hydraulic properties are provided by the international UNSODA database (Leij et al., 1996). Key parameters include: $k = 1 \times 10-6$ m/s, $\alpha_s = 0.363$, $\alpha_r = 0.186$, and n = 1.53. The model consists of a vertical soil column (1 m thickness) with an initial pressure head of -8 m across the domain. The top boundary is set to a pressure head of 0 m to simulate free surface infiltration.

Case 2: A 2D laboratory infiltration experiment by Vauclin et al. (1979), widely used for evaluating saturated-unsaturated unsteady seepage models. The soil slab measures 2.00 m in height, 6.00 m in width, and 0.05 m in thickness, with an impermeable base and free drainage boundaries on both sides. Initially, the water table is set at 0.65 m. A central 1.00 m section of the top boundary receives uniform precipitation at 0.148 m/h for 8 hours, during which free surface evolution is monitored. Soil hydraulic properties are described using the van Genuchten-Mualem model with parameters: $k = 0.35 \, m/h$, $\alpha_s = 0.30$, $\alpha_r = 0.01$. Due to symmetry, the DBS model simulates the right half of the domain."

Lines 281-291:

"2.3 CFPv2 model

The CFPv2 model, proposed by Reimann et al. (2014), is an advanced version of MODFLOW-CFP (Shoemaker et al., 2008). It extends functionalities such as flow interactions between conduits and porous media, as well as conduit boundary conditions. CFPv2 integrates with MODFLOW-2005 and employs the following approaches: Laminar Flow in Conduits: Described using the Hagen-Poiseuille equation for discrete conduits within conduit networks. Turbulent Flow: Calculated by combining the Darcy-Weisbach equation with the Colebrook-White equation. Laminar Flow in Fractured Rock Matrix: Simulated via a continuum approach. Detailed technical documentation for MODFLOW-CFP, including groundwater flow simulation methodologies, is provided by Shoemaker et al. (2008). Successful applications and evaluations of the model have been reported in studies such as Gallegos et al. (2013), Reimann et al. (2014), Chang et al. (2020), Gao et al. (2020), and Shirafkan et al. (2023)."

(4) line 165: wrong unit of measure for permeability, gravitational acceleration

Thank you for your revision suggestions. We have corrected the labeling errors in the revised manuscript.

(5) line 205: delete ripetitive title

Thank you for your comments. We have removed the duplicate headings in the revised manuscript.

(6) Figure 1: insert letters a and b also in the figure for better readibility

Sincere thanks for your valuable suggestions, which are crucial for improving the quality of the paper. We have clearly labeled subplots (a), (b), (a.1), and (b.1) in Fig. 1 and updated the captions (Lines 1012–1019) to enhance readability.

Lines 1028-1035:

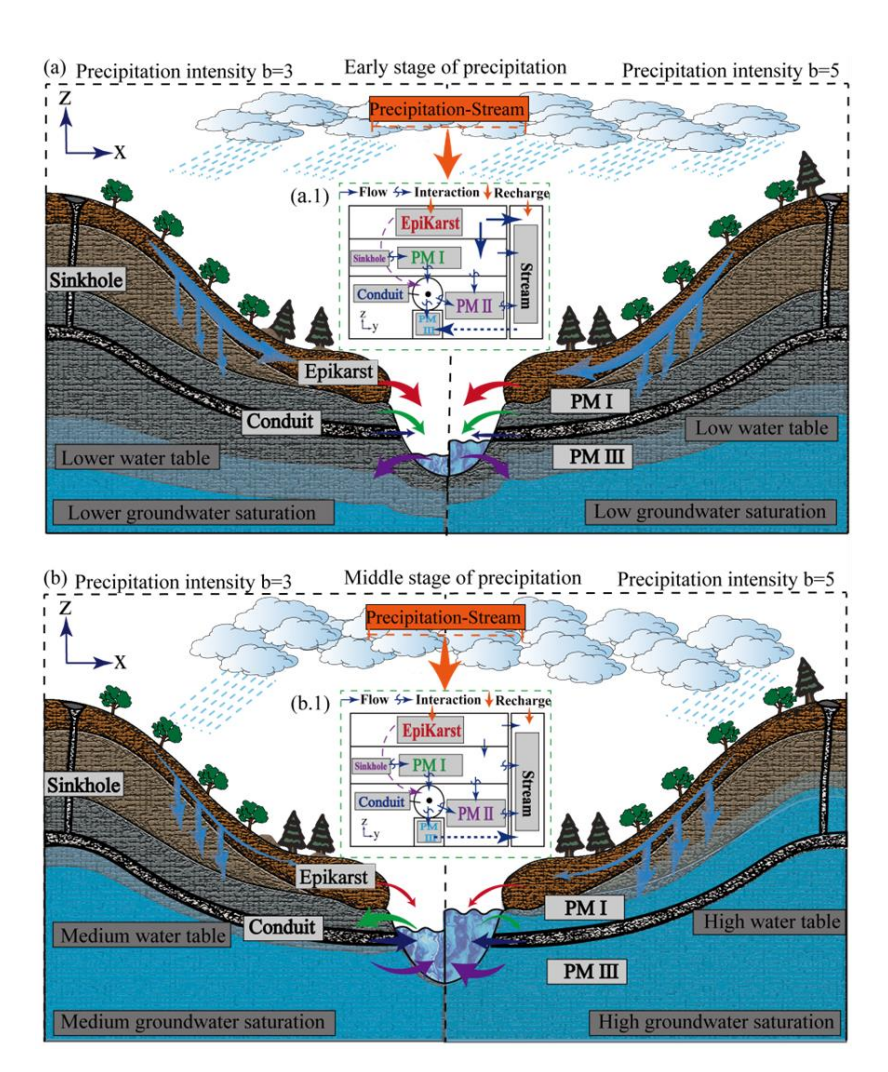


Figure 1. Schematic diagrams of the modelling of the interaction between the karst aquifer (epikarst, sinkhole, karst conduit, PM I, PM II, and PM III) and stream under dimensionless precipitation intensities (b = 3 and b = 5). (a) and (a.1) Schematic diagram of the interaction flow between each medium and stream in the early stage of a precipitation event; (b) and (b.1) Schematic diagram of the interaction flow between each medium and stream in the middle stage of a precipitation event. The size of the arrows represents the magnitude of the flow rate, and the direction of the arrows represents the direction between the two.

(7) Line 98-100: Can be revised to make it simple.

Sincere thanks for your valuable suggestions. We have simplified the descriptions in the revised manuscript.

Lines 95-97:

"(1) The Navier-Stokes (N-S) equations combined with the Darcy equation can effectively couple free flow and seepage processes (Soulaine and Tchelepi, 2016; Carrillo et al., 2020; You and Lee, 2021)."

Reply to Referee #2:

Dear Reviewer: Thank you for your comments. Our responses to the comments are listed below:

General Comments:

This manuscript presents a coupled Darcy-Brinkman-Stokes (DBS) model to simulate karst aquifer and stream interactions under various precipitation conditions, comparing its results to MODFLOW-CFP. The study is technically sound, and the modeling framework has clear potential for advancing process-based simulation of turbulent flows and unsaturated conditions in karst systems. However, the manuscript currently suffers from significant shortcomings in clarity, structure, model transparency, and broader contextual discussion. These issues limit its accessibility and impact.

Sincere appreciation for your recognition of the model framework and constructive feedback on improving the manuscript! We have thoroughly revised the content, with specific details outlined as follows:

(1) A clearer articulation of the research gap and contributions in the Introduction.

Sincere thanks for your comments. We have supplemented the research gap and this study's contributions in the Introduction section:

- Clarified research gaps: Noted limitations of CFPv2 (single-phase flow only) and Hydrus (difficulty in coupling conduit flow) (Lines 78–80, 90–92), highlighting the innovation of the DBS model in fully coupling two-phase flow, variably saturated flow, and turbulent flow (Lines 99–105).
- Enhanced contribution statements: Added a concluding paragraph (Lines 113–119) emphasizing the model's breakthrough in resolving karst aquifer-stream combined recharge mechanisms.

(2) A reorganization and simplification of the Methods section, with better-defined subsections and clearly stated variable definitions.

Thank you for your comments. We have revised the Methodology section and provided a variable definition table.

- Structural adjustments: Reorganized into subsections 2.1–2.5 (including the variable definition table, lines 1019-1020) to enhance logical clarity.
- Clarification of key concepts: Added justification for turbulence simulation (lines 219-223), definition of two-phase flow parameters (lines 180-203), and the rationale for selecting the VGM/BC models (lines 252-279).

(3) Improved figure quality and more structured result narratives that highlight key trends, comparisons, and implications.

Thank you for your comments. In the revised manuscript, we have reorganized the results section and included a comparison of CFPv2 with our study.

(4) A more rigorous and quantitative comparison with MODFLOW-CFP, beyond qualitative differences.

Thank you for your comments. In the revised manuscript, we have conducted a quantitative comparison between CFPv2 and the DBS study, and provided a quantitative comparison table.

- Quantitative comparison with CFPv2: Added Table 3 (line 1025) comparing metrics such as peak discharge and peak arrival time to clarify the advantages of the DBS in capturing double flood peaks.
- (5) A deeper discussion of how the findings contribute to our understanding of karst-stream interactions and why this modeling advance matters in practice.

Thank you for your comments. In the revised manuscript, we have elaborated on the contribution of the DBS model to flood prevention and mitigation under karst-stream interactions.

• Enhanced practical significance: Expanded the analysis of the model's potential in flood warning systems (lines 781-792) and water resource allocation optimization.

Specific Comments Title

- (6) The current title is vague and lacks specificity about the method or novelty.
 - Consider revising to reflect the modeling framework or scientific contribution, e.g., "Simulating Precipitation-Induced Karst-Stream Interactions Using a Coupled Darcy-Brinkman-Stokes Model".

Thank you for your comments. We have revised the title in the updated manuscript.

• Lines 1-2: "Simulating Precipitation-Induced Karst-Stream Interactions Using a Coupled Darcy-Brinkman-Stokes Model."

Abstract:

(7) Long abstract detracts from its purpose, it should be short and to the point.

In the revised manuscript, we have condensed the abstract length and clarified the main focus of the paper.

Lines 13-39:

"Abstract. The variation in seasonal precipitation intensity impacts the dynamic interaction between the karst aguifer and stream. However, the interaction mechanism between the karst aquifer and stream is currently still unclear, and characterizing the impact of dynamic saturation process of groundwater in karst media on the interaction process remains a challenge. This study provides an in-depth analysis of the interaction processes between karst aguifer systems and adjacent streams, along with water-air two-phase flow in aquifer media. Multiple water retention models were employed to characterize the soil-water characteristics of porous media and variably saturated groundwater flow. The research reveals that rainfall intensity variations significantly influence the interactions between karst aquifer systems and streams. These interactive processes become increasingly complex with higher rainfall intensities, involving multi-media collaborative recharge and dynamic interactions, while the contribution proportions of different media to streamflow also change accordingly. By comparing the modeling differences and numerical results between CFPv2 and DBS approaches in generalized models, the validity of the DBS model for groundwater modeling was verified. Under consecutive rainfall events, total rainfall intensity plays a crucial role in hydrological process variations of adjacent streams. Groundwater stored in porous media of karst systems during the first rainfall event was found to influence stream water levels during subsequent rainfall events, while conduit storage exhibited minimal impact. Multi-level conduit configurations under specific conditions, particularly during intense rainfall, can significantly affect hydrological processes in both streams and karst conduits. Uncertainty analysis demonstrates that conduit geometry, diameter, epikarst permeability, and porosity differentially influence hydrological processes in karst aquifer systems. Variations in these parameters induce corresponding changes in peak flow rates, peak timing of stream and karst spring discharges, as well as redistribution of discharge contributions among different media, ultimately affecting the overall hydrological dynamics of the coupled karst aquifer-stream system. It can accurately depict the two-phase interactive flow between various media controlled by the dynamic saturation process, and reveal the dynamic interaction process between karst aguifers affected by the epikarst, sinkholes, and conduits under infiltration recharge and stream. Meanwhile, it can precisely explain the processes of infiltration, overflow, and recession."

(8) Avoid referring to equation names (e.g., DBS, BC, VGM) without explanation. Focus on what was learned, not just what was done.

Thank you for your comments. We have rewritten the abstract in the revised manuscript to avoid direct reference to equations.

Introduction:

(9) Introduce a clear knowledge gap: why are existing models insufficient?

In the revised manuscript, we have clarified the rationale for employing the Darcy-Brinkman-Stokes (DBS) model based on the following key points:

- Applicability Limitations of MODFLOW-CFP: The applicability of MODFLOW-CFP is limited by its current capability to simulate only single-phase flow (Lines 78-80).
- Inherent Difficulties with Hydrus: The Hydrus model faces inherent difficulties in coupling rapid conduit free flow with porous media seepage flow in karst regions, due to its lack of a specialized conduit flow solution (Lines 90-92).
- Advantages of the DBS Model: In contrast, the DBS model emerges as an ideal choice for simulating the complex flow within karst systems (including saturated-unsaturated two-phase flow) because of its theoretical foundation for coupling free flow and seepage flow within a unified framework. Multiple recent studies cited in Lines 99-105 (Huang et al., 2024; Nillama et al., 2022; Carrillo et al., 2020; Lu et al., 2023; Soulaine, 2024) adequately demonstrate the effectiveness and potential of the DBS approach in characterizing the coupled processes of conduit/fracture flow and matrix seepage flow.

Lines 78-80:

"Although MODFLOW-CFP is relatively comprehensive for regional karst groundwater simulation studies, the current version of MODFLOW-CFP only supports modeling single-phase groundwater flow."

Lines 90-92:

"However, this approach lacks a built-in conduit flow solution scheme, making it difficult to adequately address the coupling requirements between rapid conduit flow and porous media seepage in karst areas."

Lines 99-105:

"The Darcy-Brinkman-Stokes equations have been utilized to couple seepage flow and free flow (Huang et al., 2024; Nillama et al., 2022; Carrillo et al., 2020). Lu et al. (2023) analyzed a model that integrates fast discharge channels in fractures and conduits with slow seepage in porous media. The results demonstrate that the Darcy-Brinkman-Stokes equations can effectively describe two-phase flow in karst aquifers, and Soulaine (2024) proposed that mixed-scale models based on the Darcy-Brinkman-Stokes equations have strong potential for simulating coupled processes in porous systems."

(10) State specific objectives and contributions at the end of the introduction.

We added the following statement at the end of the Introduction (Lines 113-119):

"The DBS model represents the first implementation enabling the fully coupled simulation of twophase flow, variably saturated conditions, and turbulent flow within karst systems. This addresses a gap in existing tools (e.g., CFPv2), which cannot characterize the dynamic, synchronized recharge processes involving saturation changes."

Lines 113-119:

"This study aims to employ a two-phase variably saturated model capable of coupling free flow and seepage flow to reveal the interaction mechanisms between the karst aquifer system and adjacent stream under rainfall infiltration recharge-driven conditions. Specifically, it focuses on further investigating how groundwater saturation variations in different media (e.g., conduits, fractures, matrix) of the karst aquifer system influence inter-media interactions. This research addresses the gap in existing studies where current numerical methods struggle to accurately characterize the collaborative recharge processes among various media within karst aquifer systems."

(11) Consider breaking the introduction into shorter paragraphs or subsections.

We thank the reviewer for the comment. In the revised manuscript, we have divided the longer paragraphs to enhance readability.

Methods:

(12) The modeling section is too dense and difficult to follow.

We appreciate your valuable feedback. In the revised manuscript, we have thoroughly restructured the Methods section as follows:

2. Materials and methods

2.1 Numerical modelling

2.2 DBS model

- 2.2.1 Two-Phase Flow Parameter Definition
- 2.2.2 Governing Equations
- 2.2.3 Subdomain Formulation
- 2.2.4 Relative Permeability Model

2.3 CFPv2 model

2.4 Model Comparison and Numerical Model Construction

2.4.1 DBS Model Conversion and Applicability Assessment

2.4.2 Model Comparison and Discretization Schemes

2.5 Rainfall Infiltration Recharge Boundary

(13) Key concepts (e.g., turbulent conduit flow, two-phase flow, saturation) are introduced without sufficient explanation.

We appreciate your feedback. In the revised manuscript, we have provided clearer explanations of turbulent conduit flow, two-phase flow, and saturation dynamics before reintroducing these concepts.

Lines 219-233:

"Conduit networks in karst aquifer systems are often associated with turbulent flow (Reimann et al., 2011). To resolve turbulence in the DBS (Dual-domain Brinkman-Stokes) equations, the Unsteady Reynolds-Averaged Navier-Stokes (URANS) framework is required. As demonstrated by del Jesus et al. (2012), the k-epsilon turbulence model is effective for evaluating turbulent processes within porous media. Consequently, the k-epsilon-based DBS turbulence governing equations are formulated as follows:

$$\nabla \cdot v_t = 0 \tag{2}$$

$$\frac{\partial \varphi \alpha_l}{\partial t} + \nabla \cdot (\alpha_l v_t) + \nabla \cdot (\varphi \alpha_l \alpha_g v_{rt}) = 0 \tag{3}$$

$$\frac{1}{\varphi} \left((1+c) \frac{\partial \rho v_t}{\partial t} + \nabla \cdot \left(\frac{\rho}{\varphi} v_t v_t \right) \right) =$$

$$-\nabla p^* + \rho g \cdot X + \nabla \cdot \left(\mu_{eff} (\nabla v_t + \nabla v_t^T) \right) - \mu_{eff} k^{-1} v_t + F_c.$$
(4)

where, v_t represents the turbulent velocity vector [L/T], v_{rt} is the relative velocity of gas-phase and water-phase turbulence [L/T], and μ_{eff} is the effective viscosity, which can be defined as $\mu_{eff} = \mu + \rho v_{turb}$, where μ is the dynamic viscosity and v_{turb} is the turbulent kinetic viscosity.

The eddy viscosity is expressed as:

$$\mu_t = \rho C_\mu \frac{k_t^2}{\varepsilon} \tag{5}$$

where: k_t : Turbulent kinetic energy per unit mass $[m^2/s^2]$, ε : Turbulent dissipation rate per unit mass $[m^2/s^3]$, C_u : Dimensionless constant with a value of 0.09."

Lines 180-203:

"2.2.1 Two-Phase Flow Parameter Definition

Assuming that gas and liquid fill the solid pore space, porosity is defined to characterize the percentage of the gas and liquid phases occupying the total pore space.

$$\varphi = \frac{V_l + V_g}{V} \tag{6}$$

In this context, φ represents porosity, V denotes the total volume of the unit $[m^3]$, while V_l and V_g correspond to the volumes of the liquid phase (water) and gas phase (air), respectively $[m^3]$.

Hirt and Nichols (1981) introduced the Volume of Fluid (VOF) method, which employs an additional governing equation to capture fluid motion at free surfaces. Furthermore, the saturation of each phase in the fluid is defined as α_i , where:

Liquid phase saturation: $\alpha_l = \frac{V_l}{V_g + V_l}$.

Gas phase saturation: $\alpha_g = \frac{V_g}{V_g + V_l}$.

Here, the subscripts l and g denote water and air, respectively. Thus, the spatial distribution of water and gas within the porous medium is characterized by porosity φ and phase saturation α_l :

$$\varphi = \begin{cases}
1 & \text{free regions} \\
0 < \alpha < 1 & \text{porous regions} \\
0 & \text{solid regions}
\end{cases}$$
(7)

$$\alpha_l = \begin{cases} 1 & \text{water} \\ 0 < \alpha < 1 & \text{two-phase zone} \\ 0 & \text{air} \end{cases}$$
 (8)

The average fluid density $\rho[m^3/kg]$ and viscosity $\mu[m^2/s]$ within a grid cell are calculated via saturation-weighted averaging:

$$\rho = \rho_g \alpha_g + \rho_l \alpha_l \tag{9}$$

$$\mu = \alpha_g \mu_g + \alpha_l \mu_l \tag{10}$$

where ρ_g is the gas phase density [m³ /kg] and ρ_l is the liquid phase (water) density [m³ /kg].

The transport equation for saturation α_i , following Rusche (2002), is expressed as:

$$\frac{\partial \varphi \alpha_l}{\partial t} + \nabla \cdot (\alpha_l v_t) + \nabla \cdot (\varphi \alpha_l \alpha_g v_{rt}) = 0 \tag{11}$$

where: v_t is the fluid velocity vector [m/s], v_{rt} is the relative velocity between the gas and liquid phases [m/s]."

(14) Variables are often undefined or defined long after their use.

We appreciate your comment. In the revised manuscript, we have carefully refined the definitions of key variables to improve clarity and precision.

(15) Provide a table of variable definitions.

We appreciate your comment. In the revised manuscript, we have included a comprehensive variable definition table (see Table 1) to clarify all key parameters and their respective units.

Lines 1019-1020:

Table 1: Variable Definition Table

φ Porosity field	
77 1 04 ' 1	
V Volume of the averaging-volume	m^3
V _l Water Volume	m^3
V_g Gas Volume	m^3
α_l Water Saturation	
α_g Gas Saturation	
$\alpha_{l, e}$ Effective Saturation	
ρ Average Fluid Density	kg/m^3
$ ho_g$ Gas Density	kg/m^3
$ ho_l$ Water Density	kg/m^3
μ Viscosity	$Pa \cdot s$
μ_g Gas Viscosity	$Pa \cdot s$
μ_l Water Viscosity	$Pa \cdot s$
μ_{eff} effective viscosity	$Pa \cdot s$
\overline{v} velocity	m/s
$\overline{v_r}$ relative flow rate of the gas phase to the liquid phase	e m/s
v_t turbulent velocity vector	m/s
v_{rt} relative velocity of gas-phase and water-phase turbuler	nce m/s
v_{turb} turbulent kinetic viscosity	m^2/s
$ar{p}$ pressure	Pa
p^* pressure	Pa
F_c Surface tension force	N
S_f Drag Source Term	N/m^3
C_{μ} Dimensionless Constant	
k _t Turbulent Kinetic Energy	m^2/s^2
ε Turbulent Dissipation	m^2/s^3

k	Apparent permeability	m^2
k_0	Absolute permeability	m^2
k_{rg}	Gas Relative Permeability	
k_{rl}	Water Relative Permeability	
g	Gravitational Acceleration	m/s^2
X	position vectors in Cartesian	
σ	Interfacial tension	N/m
p_c	Capillary pressure	Pa
n	Brooks and Corey Coefficient	
m	Van Genuchten Coefficient	

(16) Clearly justify modeling choices: Why use turbulence? Why VGM vs. BC?

We appreciate your feedback. In the revised manuscript:

- Regarding turbulence justification
 We have clarified the rationale for selecting turbulent flow modeling (Lines 219-223).
- Concerning VGM vs. BC model comparison
 We now provide a parallel analysis of both the VGM and BC models, with specific
 discussion of scenarios where the VGM formulation demonstrates advantages over the
 BC approach (Lines 252-279).

Lines 219-223:

"Conduit networks in karst aquifer systems are often associated with turbulent flow (Reimann et al., 2011). To resolve turbulence in the DBS (Dual-domain Brinkman-Stokes) equations, the Unsteady Reynolds-Averaged Navier-Stokes (URANS) framework is required. As demonstrated by del Jesus et al. (2012), the k-epsilon turbulence model is effective for evaluating turbulent processes within porous media."

Lines 252-279:

"2.2.4 Relative Permeability Model

Accurate modeling of two-phase flow in porous media is critical in geosciences. Simulating two-phase flow in variably saturated porous media requires precise estimation of the relationship between relative permeability and saturation (Springer et al., 1995).

To characterize the variation in two-phase relative permeability, the effective saturation of the liquid phase must first be defined. This is expressed as:

$$\alpha_{l,e} = \frac{\alpha_l - \alpha_{l,r}}{1 - \alpha_{q,r} - \alpha_{l,r}} \tag{12}$$

where: $\alpha_{l,e}$ denotes the effective water saturation, α_l and $\alpha_{l,r}$ represent the water saturation and residual water saturation, respectively, and $\alpha_{q,r}$ is the residual air saturation.

Relative permeability is a critical parameter in groundwater and related engineering fields (Kuang and Jiao, 2011). The Brooks and Corey (BC) model (Brooks and Corey, 1964) and the van Genuchten model (van Genuchten, 1980) are widely used as representative relative permeability models. The BC model establishes a relationship between relative permeability and effective water saturation as follows:

$$k_{rg} = \left(1 - \alpha_{l, e}\right)^n \tag{13}$$

$$k_{rl} = \alpha_{l,e}^n \tag{14}$$

 k_r denotes the relative permeability, where n is a dimensionless coefficient determined by the properties of the porous medium. The Brooks-Corey (BC) model exhibits a sharp discontinuity at the air entry point, which can lead to poor data fitting, particularly for fine-textured soils (Assouline & Or, 2013). The van Genuchten (1980) model addresses this limitation. By incorporating the parameter m = 1 - 1/n proposed by Mualem (1976), the modified van Genuchten-Mualem (VGM) model (Parker et al., 1987) is formulated as:

$$k_{r,g} = \left(1 - \alpha_{l,e}\right)^{0.5} \left(1 - \alpha_{l,e}^{1/m}\right)^{2m} \tag{15}$$

$$k_{r,l} = \alpha_{l,e}^{0.5} \left(1 - \left(1 - \alpha_{l,e}^{1/m} \right)^m \right)^2 \tag{16}$$

Here, m is a dimensionless parameter.

The selection of permeability equations is critical for appropriate predictions of relative permeability (Yang et al., 2019), indicating that pore tortuosity-connectivity plays a dominant role in groundwater two-phase flow. Therefore, this study conducts simulations and parameter sensitivity analyses for both the Brooks-Corey (BC) and van Genuchten-Mualem (VGM) models."

Results:

(17) The results are structured around simulations but lack comparative synthesis. Each simulation is described in isolation.

We appreciate your feedback. In the revised manuscript, we have restructured the Results section according to the following framework:

3. Results

- 3.1 Interaction process between the karst aquifer and stream under precipitation infiltration recharge
 - 3.1.1 Karst Aquifer-Stream Interactions Under Varying Precipitation Intensities
- 3.1.2 Interaction process between the karst aquifer and stream during early stage of precipitation
- 3.1.3 Interaction process between the karst aquifer and stream during early stage of precipitation
- 3.2. Impact of multiple precipitation events on the interaction process between the karst aquifer and stream
- 3.3. Effects of Water Retention Characteristics on Karst Aquifer-Stream Interactions
- 3.4. Impact of multi-stage permeability and porosity arrangement on the interaction process between the karst aquifer and stream

(18) Start each subsection with a motivating question (e.g., "How does conduit depth affect stream discharge?").

We appreciate your insightful observation regarding the value of engaging questions. In the revised manuscript, we have implemented the following enhancements to improve reader engagement:

Lines 478-480:

"How does the threshold attainment of storage capacity in the lower porous media affect the hydrological processes of the upper porous media?"

Lines 547-549:

"Does the groundwater stored in the porous media of the karst aquifer system during the initial rainfall event influence the interactions between multi-component media during subsequent precipitation episodes?"

(19) Emphasize key differences in system behavior (e.g., thresholds, flow reversals, saturation delays).

Thank you for your comments. We have actively incorporated your suggestions in the revised manuscript to analyze key systematic differences.

(20) Integrate comparisons to MODFLOW-CFP throughout instead of relegating to the end.

We have conducted a comparative analysis between DBS and CFPv2 in the section preceding the two-phase flow results.

Comparison with MODFLOW-CFP:

Lines 410-424:

"Based on the comparison between DBS and Modflow-CFPv2 results in Figs 4(a), (b), and (c), the CFPv2 model exhibits a single-peak hydrograph with exponential recession characteristics, failing to capture flow process line disturbances caused by multi-media interactions. Under precipitation intensities b=3 and 5, the CFPv2 model shows an immediate rapid increase in stream discharge during early stages rather than gradual enhancement, though total discharge and baseflow during later stages remain comparable (as shown in Table 3). Specifically, for b=3, the peak stream discharge in Modflow-CFPv2 occurs at 2520 s, earlier than in the DBS model. This discrepancy arises because the precipitation recharge package in CFPv2 directly elevates water levels, whereas the DBS model simulates a gradual vertical infiltration process along the Z-axis. Lower precipitation intensity reduces groundwater infiltration rates and prolongs water table replenishment time, consequently delaying lateral discharge timing. At b=7, both models exhibit comparable first discharge peaks, but the DBS model generates a secondary peak through overflow effects that rapidly recedes after overflow cessation. In contrast, CFPv2 demonstrates smooth exponential recession without secondary features due to its simplified vertical stratification that neglects multi-component interactions."

(21) The comparison is largely qualitative.

Thank you for your comments. We have added quantitative comparisons in the revised manuscript.

- Add quantitative metrics (e.g., time to saturation, max stream recharge, total outflow). We have supplemented relevant quantitative metrics in the revised manuscript. Peak Lag Time (s); Peak Flow (m³/s); Total Outflow (m³)
 - Include a summary table comparing DBS and MODFLOW results for key variables.

Added Table 3 (Line 1025) with quantitative comparisons of key metrics (time-to-peak, peak discharge, total outflow), demonstrating that the DBS model effectively captures complex processes such as secondary flood peaks (which CFPv2 overlooks due to its simplified vertical layering). This highlights DBS's superior capability in characterizing multi-media interactions.

Numerical Model	Peak Lag Time (s)		Peak Flow (m^3/s)			Total Outflow (m^3)			
	b=3	b = 5	b = 7	<i>b</i> = 3	b = 5	b = 7	b=3	b = 5	b = 7
DBS Model	3242. 96	1870. 18	2985. 31	4.50	12.14	21.96	65984 .49	15415 8.46	27294 5.87
MODFLO W-CFPv2	2520. 00	1920. 00	1860. 00	4.31	11.87	18.87	63916 .15	15754 3.65	24551 9.26

Table 3: Comparing DBS and MODFLOW results for key variables

(22) Discuss the limitations of MODFLOW-CFP more directly — why does it fail to simulate certain behaviors?

Thank you for your comments.

- The DBS model successfully captured the secondary flood peak overlooked by CFPv2, revealing a multi-media synergistic recharge mechanism.
- CFPv2 failed to simulate the overflow-driven secondary flood peak (Fig. 3) due to its simplified vertical layering (1D conduit flow), whereas DBS overcame this limitation through coupled 3D conduit flow modeling.

Lines 301-303:

"However, the DBS model operates in three dimensions (3D), requiring grid refinement around conduits and their vicinity to ensure accurate flow resolution. This increases computational load compared to the 1D conduit flow framework of CFPv2."

Lines 1036-1040:

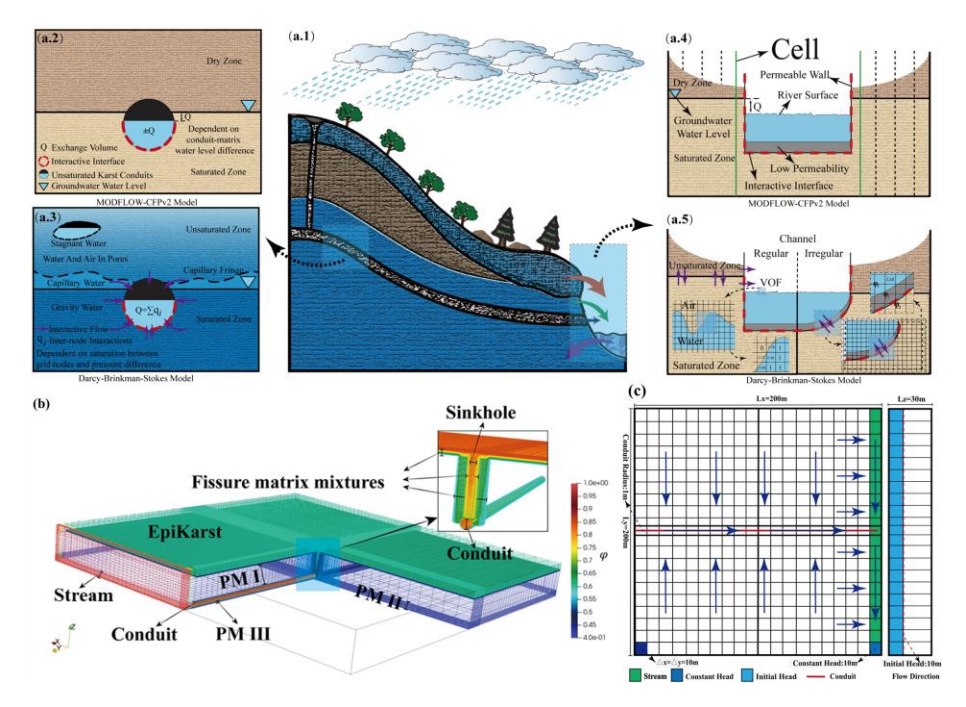


Figure 3. (a) Schematic comparison of conduit and porous media coupling modes between MODFLOW-CFPv2 and DBS, (b) DBS model and (c) CFPv2 discretization schemes for karst aquifer systems with riverside models.

Discussion:

(23) The discussion largely restates results and does not engage deeply with broader hydrologic or modeling implications.

Thank you for your comments. We have reorganized the results in the Discussion section and further investigated the influence of sensitivity parameters on the modeling:

• Address: What do these findings imply about karst vulnerability under extreme precipitation?

• Discuss potential applications of the DBS model in field calibration, water management, or integrated modeling platforms.

Thank you for pointing out the need to strengthen the connection to practical applications in the Discussion section. In the revised manuscript, we have supplemented the implications of modeling parameters for water resource management in karst areas, including the vulnerability of karst systems under extreme precipitation events using the DBS model, and its potential applications in water resource management or integrated modeling platforms:

- Lines 725-731: Discusses the impact of conduit geometry (e.g., square cross-section) on aquifer-stream exchange fluxes, emphasizing its key role in enhancing simulation accuracy.
- Lines 756-763: Analyzes how epikarst permeability governs groundwater flow paths, illustrating the importance of parameter calibration for water resource predictions.
- Lines 781-792: Adds an analysis of the influence of porosity parameters on karst water resource allocation and geological stability, clarifying the model's potential applications in flood early warning systems.

Lines 725-731:

"Conduit geometry (radius and shape) constitutes a critical factor in karst aquifer hydrological modeling. Larger circular conduits accelerate peak discharge arrival and amplify stream-connected flow peaks and karst spring discharge. Square-section conduits outperform circular equivalents in peak discharge capacity under identical nominal radii due to cross-sectional area advantages. Enlarged conduits intensify porous medium-stream interactions and amplify PM III recharge through gravitational effects. Comprehensive consideration of conduit geometry impacts on hydrological elements is essential for improving model accuracy and reliability in simulating karst aquifer-stream interaction processes."

Lines 756-763:

"Epikarst permeability constitutes a critical factor in hydrological modeling of karst aquifer systems. Highly permeable epikarst produces rapid streamflow peaks followed by sharp declines, reflecting efficient groundwater leakage to the stream. Conversely, low permeability yields diminished peaks and broader discharge curves. While karst spring discharge remains relatively stable when epikarst permeability differs from porous media, proper characterization of epikarst permeability is essential for accurately simulating hydraulic interactions between media, regulating groundwater flow pathways and velocities. This enhances model reliability in capturing complex flow dynamics within karst conduit-stream systems."

Lines 781-792:

"In hydrological modeling, porosity parameters must be calibrated to accurately simulate groundwater flow paths and storage-release dynamics. For low-porosity regions, models should emphasize rapid drainage capacity of conduit systems and transient flow variations. In highporosity areas, considerations should include fluid retention risks, stream-porous media interactions, and their long-term impacts on geological stability and water resource allocation. Proper porosity parameterization enhances simulation accuracy for diverse hydrological processes, enabling improved prediction and management of karst water resources.

Karst hydrological vulnerability manifests prominently through rapid infiltration, epikarst runoff, groundwater table fluctuations, and abrupt spring discharge variations. The DBS model effectively simulates multi-media interactions during extreme recharge events, enabling temporal analysis of media-stream exchanges, identification of peak interaction values, and applications in coupled conduit flow-seepage processes for two-phase flow systems."

(24) Compare to other recent modeling studies in karst hydrology (e.g., those using HYDRUS, ParFlow, or CFP enhancements).

Thank you for your comments. We first replaced the comparative CFP model with the updated CFPv2 model and added two references for comparative validation.

- Literature Comparison: Added quantitative validation against experimental data from Warrick et al. (1985) and Vauclin et al. (1979) (lines 614-633), demonstrating the reliability of the DBS model in simulating variably saturated flow.
- Model Comparison: Compared the DBS model with the enhanced CFP version (MODFLOW-CFPv2) (lines 301-303), and expanded the explanation of CFPv2 principles in the "Methods" section (lines 280-291). (29)

Missing Elements:

(25) Model Validation: No benchmark or field validation is presented — even conceptual model validation would strengthen the work.

Thank you for your comments. We conducted comparative validation of the model using two published studies.

• Literature Comparison: Added quantitative validation against experimental data from Warrick et al. (1985) and Vauclin et al. (1979) (lines 614-633), demonstrating the reliability of the DBS model in simulating variably saturated flow.

(26) Uncertainty Analysis: Sensitivity to soil properties, precipitation rate, conduit geometry, etc., is not discussed.

Thank you for your comments. The revised manuscript discusses sensitivity analyses and potential impacts of soil properties, conduit size, conduit shape, porosity, and permeability:

- A new "4. Uncertainty Analysis" section (lines 693-792) demonstrates that:
- (1) Conduit geometry (square sections yield higher peak flows than circular ones)

(2) Permeability of the epikarst zone (higher permeability enhances inter-media exchange frequency)

are key factors regulating karst-stream feedback mechanisms. This provides prioritization guidance for model parameter calibration.

4. Uncertainty Analysis and Discussion

The multi-level conduit configuration inherently affects multi-media interactions by simultaneously altering permeability, conduit diameter, and porosity parameters. This study will further conduct sensitivity analyses on individual variables to investigate their impacts on the vulnerability of karst aquifer systems.

4.1 Impacts of Conduit Diameter and Geometry on Interactions Between Karst Aquifer Systems and Streams

Fig. 12 presents hydrographs under conditions of circular conduits with varying radii (r=0.2, 0.3, 0.3, and 0.5 m) and square-section conduits (r=0.5 m) for (a) stream-connected flow, (b) karst spring discharge, (c) epikarst flow, (d) porous medium I (PM I), (e) PM II, and (f) PM III. Fig. 12(c.1) illustrates different conduit cross-sectional shapes to analyze their impacts on the interactive flow between karst aquifer systems and adjacent streams.

As shown in Fig. 12(a), larger conduit radii correspond to higher initial discharge peaks and shorter peak arrival times, indicating enhanced porous medium recharge and faster fluid transmission through larger conduits. Notably, the square-section conduit (s-r_c=0.5) exhibits higher peak discharge than its circular counterpart (rc=0.5) due to its surplus cross-sectional area accommodating greater fluid discharge under identical nominal radii.

Fig. 12(b) demonstrates that karst spring peak discharge increases with conduit radius. At r=0.5 m, the square-section conduit ($s-r_c=0.5$) achieves higher peak discharge than the circular conduit ($r_c=0.5$), but displays lower recession flow. This occurs because identical precipitation infiltration recharge leads to greater porous medium storage depletion during peak periods in square conduits, subsequently reducing porous medium-to-conduit recharge during baseflow recession.

Combined analysis of Figs. 12(c), (d), and (e) reveals that conduit radius variations do not significantly affect epikarst hydrographs or PM I/II hydrographs. However, square-section sinkholes modify flow patterns: epikarst hydrographs show lower values under square conduits, while PM I/II hydrographs exhibit higher values due to enhanced epikarst groundwater collection in square cross-sections, increasing recharge to PM I/II.

Fig. 12(e) indicates that larger conduit radii correspond to lower negative values. Combined with Fig. 12(a), this demonstrates that increased stream recharge through larger conduits elevates both stream peak discharge and water levels, thereby enhancing porous medium-stream interactions. Similarly, Fig. 12(f) shows that larger conduit radii increase karst spring discharge and PM III hydrograph elevation through enhanced gravity-driven groundwater recharge.

Conduit geometry (radius and shape) constitutes a critical factor in karst aquifer hydrological modeling. Larger circular conduits accelerate peak discharge arrival and amplify stream-connected flow peaks and karst spring discharge. Square-section conduits outperform circular equivalents in peak discharge capacity under identical nominal radii due to cross-sectional area advantages. Enlarged conduits intensify porous medium-stream interactions and amplify PM III recharge through gravitational effects. Comprehensive consideration of conduit geometry impacts on hydrological elements is essential for improving model accuracy and reliability in simulating karst aquifer-stream interaction processes.

4.2 Influence of Permeability on the Interaction Processes Between Karst Aquifer Systems and Streams

The permeability of the epikarst directly controls the ease of fluid infiltration from the surface into the conduit system. Fig. 13 illustrates the hydrological process curves under different epikarst permeability coefficients ($K_E=10^{-6}$, 10^{-7} , 10^{-8} , 10^{-9} ; when $K_E=10^{-9}$, the permeability matches that of porous media, rendering the epikarst incapable of rapid groundwater leakage) for: (a) stream, (b) karst spring, (c) epikarst, (d) PM I, (e) PM II, and (f) PM III. This aims to reveal how epikarst permeability regulates groundwater flow patterns in complex conduit systems and intermedia interactions.

As shown in Fig. 13(a), under high epikarst permeability ($K_E=10^{-6}$): the discharge curve rises rapidly to a peak of ~4.5 m^3/s followed by a sharp decline. This indicates that high permeability enables rapid groundwater leakage from the epikarst to the stream, causing swift flow increases. Peak stream discharge diminishes with decreasing permeability. High permeability reduces flow resistance, facilitating faster fluid entry into the conduit system and generating sharp discharge peaks, while low permeability increases resistance, resulting in gradual fluid release and broader, lower discharge curves.

Fig. 13(b) demonstrates that epikarst permeability differences from porous media have minimal impact on conduit flow. However, when epikarst permeability equals that of porous media ($K_E=10^{-9}$), the peak discharge at the karst spring decreases while maintaining identical baseflow recession characteristics. Combining Figs. 13(c) and (c.1), higher epikarst permeability enhances lateral discharge to the stream. At $K_E=10^{-9}$, gravitational forces dominate vertical recharge to lower media without lateral discharge.

Fig. 13(d) reveals decreasing discharge from Porous Medium I to the stream with reduced epikarst permeability. Cross-referencing Figs. 13(a) and (e), lower epikarst permeability reduces both stream discharge and water level, limiting recharge to Porous Medium II. Fig. 13(f) shows negligible epikarst permeability influence on Porous Medium III's hydrograph.

Epikarst permeability constitutes a critical factor in hydrological modeling of karst aquifer systems. Highly permeable epikarst produces rapid streamflow peaks followed by sharp declines, reflecting efficient groundwater leakage to the stream. Conversely, low permeability yields diminished peaks and broader discharge curves. While karst spring discharge remains relatively stable when epikarst permeability differs from porous media, proper characterization of epikarst permeability is essential for accurately simulating hydraulic interactions between media,

regulating groundwater flow pathways and velocities. This enhances model reliability in capturing complex flow dynamics within karst conduit-stream systems.

4.3 Influence of Porosity on the Interaction Between Karst Aquifer Systems and Adjacent Streams

Fig. 14 presents the hydrographic process curves under different porosity conditions (φ =0.4, φ =0.3, φ =0.2, φ =0.1) for (a) stream, (b) karst spring, (c) epikarst, (d) PM I, (e) PM II, and (f) PM III. Fig. 14(c.1) illustrates the schematic diagram of groundwater flow under different pore sizes. The study aims to elucidate how porosity regulates fluid flow patterns in complex conduit systems.

As shown in Fig. 14(a), lower porosity results in higher flow peaks and earlier peak times. This occurs because reduced pore space limits groundwater storage capacity, forcing excess water to discharge rapidly and elevating the stream hydrograph. Fig. 14(b) demonstrates that lower porosity drives groundwater to preferentially flow through karst conduits and discharge at springs. In Fig. 14(c), the peak discharge of epikarst at $\varphi = 0.4$ slightly exceeds those at $\varphi = 0.3$, $\varphi = 0.2$, and $\varphi = 0.1$.

Fig. 14(d) reveals that at φ =0.1, the storage capacity of porous medium I reaches critical limits. Groundwater recharged from epikarst to porous medium I is rapidly discharged, resulting in significantly higher discharge rates compared to φ =0.3, φ =0.2, and φ =0.1. Fig. 14(e) indicates increased discharge from porous media to the stream as porosity decreases. Combined with Fig. 14(a), reduced porosity enhances stream stage and discharge but diminishes the stream's ability to recharge porous media due to limited storage capacity. Fig. 14(f) shows negligible porosity effects on the hydrograph of porous medium III, as its behavior is primarily governed by conduit flow.

In hydrological modeling, porosity parameters must be calibrated to accurately simulate groundwater flow paths and storage-release dynamics. For low-porosity regions, models should emphasize rapid drainage capacity of conduit systems and transient flow variations. In high-porosity areas, considerations should include fluid retention risks, stream-porous media interactions, and their long-term impacts on geological stability and water resource allocation. Proper porosity parameterization enhances simulation accuracy for diverse hydrological processes, enabling improved prediction and management of karst water resources.

Karst hydrological vulnerability manifests prominently through rapid infiltration, epikarst runoff, groundwater table fluctuations, and abrupt spring discharge variations. The DBS model effectively simulates multi-media interactions during extreme recharge events, enabling temporal analysis of media-stream exchanges, identification of peak interaction values, and applications in coupled conduit flow-seepage processes for two-phase flow systems."

Lines 1074-1101:

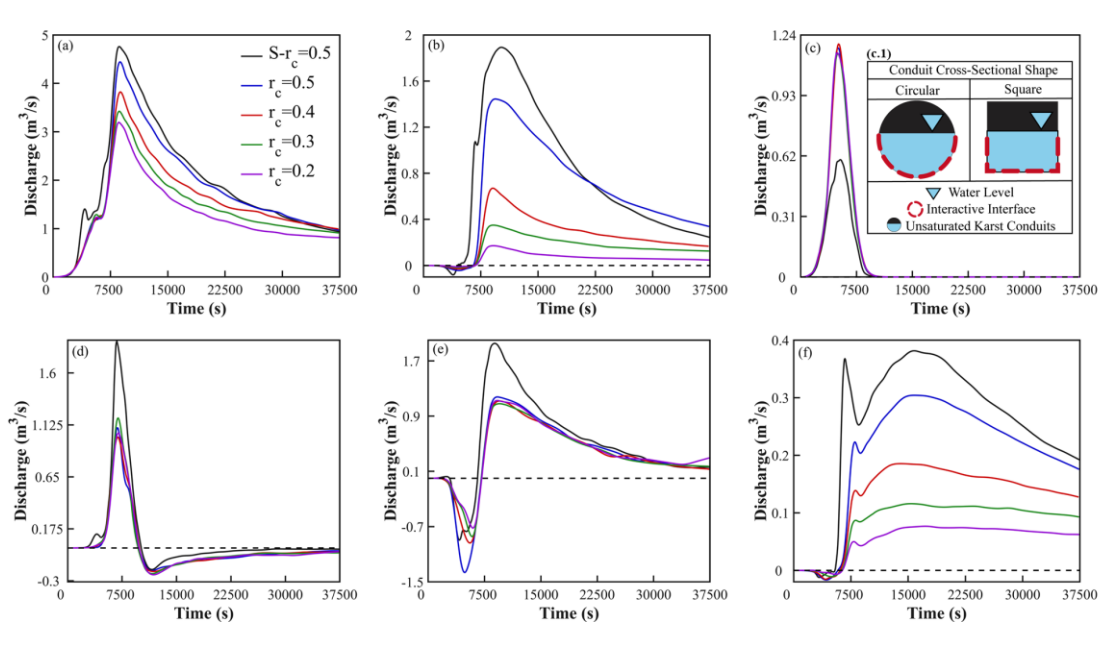


Figure 12. Hydrological process curves for (a) stream, (b) karst spring, (c) epikarst, (d) PM I, (e) PM II, and (f) PM III under conditions of circular conduits with radii $r_c = 0.2$, 0.3, 0.3, and 0.5, and square-cross-section conduits with S- $r_c = 0.5$. Subplot (c.1) shows a schematic diagram of different conduit cross-sectional shapes.

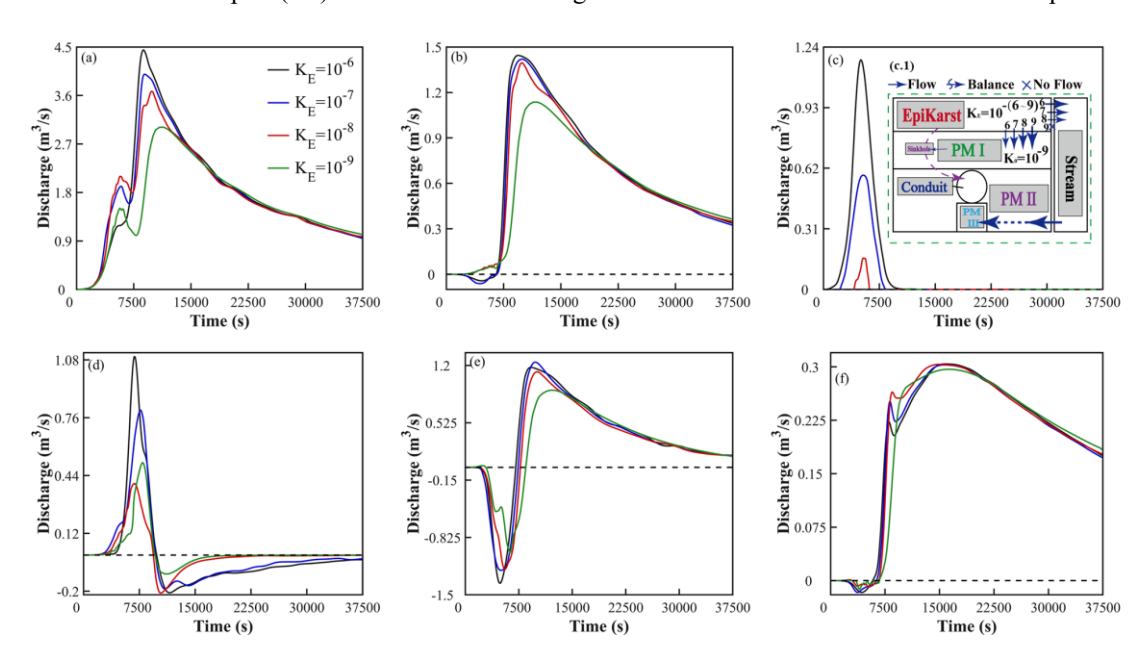


Figure 13. Hydrographs under different epikarst permeability conditions ($K_E=10^{-6}$, $K_E=10^{-7}$, $K_E=10^{-8}$, $K_E=10^{-9}$) for: (a) stream, (b) karst spring, (c) epikarst, (d) PM I, (e) PM II, (f) PM III. Subfigure (c.1) shows a schematic diagram

of media interactions under varying epikarst permeability conditions.

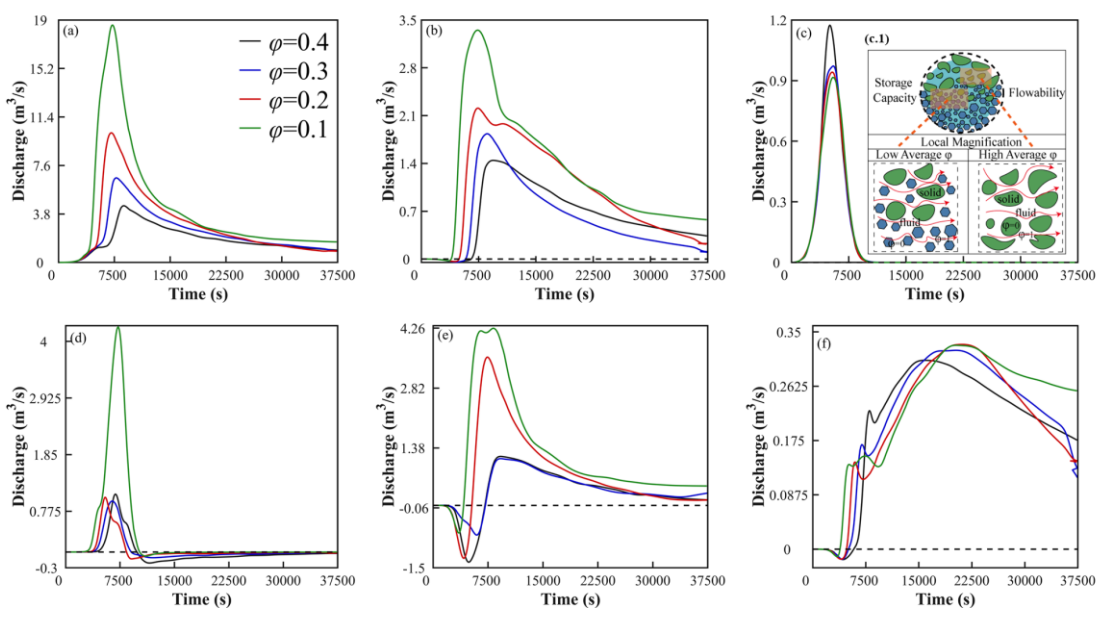


Figure 14. hydrograph curves under different porosity conditions (ϕ = 0.4, ϕ = 0.3, ϕ = 0.2, ϕ = 0.1) for (a) stream, (b) karst spring, (c) epikarst, (d) PM I, (e) PM II, and (f) PM III. Among these, (c.1) illustrates a schematic diagram of the medium's water storage capacity and flow capacity under varying porosity conditions.

Reply to Community Comment:

Thank you for your valuable comments. We have addressed each of your concerns point-by-point as follows:

(1) The authors use the Darcy-Brinkman-Stokes equations to simulate flow processes. However, further clarification on the rationale behind selecting this specific model over other commonly used approaches like MODFLOW-CFP would enhance understanding.

We sincerely appreciate your valuable suggestions, which are crucial for improving the quality of our paper. In the revised manuscript, we have clarified the rationale for selecting the DBS model: the DBS model can simulate saturated-unsaturated flow by coupling free flow and seepage flow.

Lines 78-80: "Although MODFLOW-CFP is relatively comprehensive for regional karst groundwater simulation studies, the current version of MODFLOW-CFP only supports modeling single-phase groundwater flow."

Lines 90-92: "However, this approach lacks a built-in conduit flow solution scheme, making it difficult to adequately address the coupling requirements between rapid conduit flow and porous media seepage in karst areas."

(2) Although the model captures complex interactions, the paper could benefit from a discussion of how simplifying assumptions (e.g., homogeneous permeability assumptions or simplified boundary conditions) affect the results' robustness and applicability.

We sincerely appreciate your valuable suggestions, which are instrumental in enhancing the quality of our manuscript. In the revised version, we have added a comprehensive discussion on both the advantages and limitations of the DBS model:

Lines 293-300:

"2.4.1 DBS Model Conversion and Applicability Assessment

As illustrated in Figure 2, the Navier-Stokes (N-S) model can resolve fine-scale pore-scale flows and perform high-fidelity simulations. In contrast, the CFPv2 model achieves high computational efficiency and stability by discretizing one-dimensional conduits within porous media. The DBS (Dual-domain Brinkman-Stokes) model combines the advantages of both approaches: By incorporating additional resistance source terms into the N-S equations, it maintains high-fidelity flow resolution in conduits. For porous media, it adopts a Darcy-type flow formulation, significantly reducing computational costs."

Lines 1036-1040:

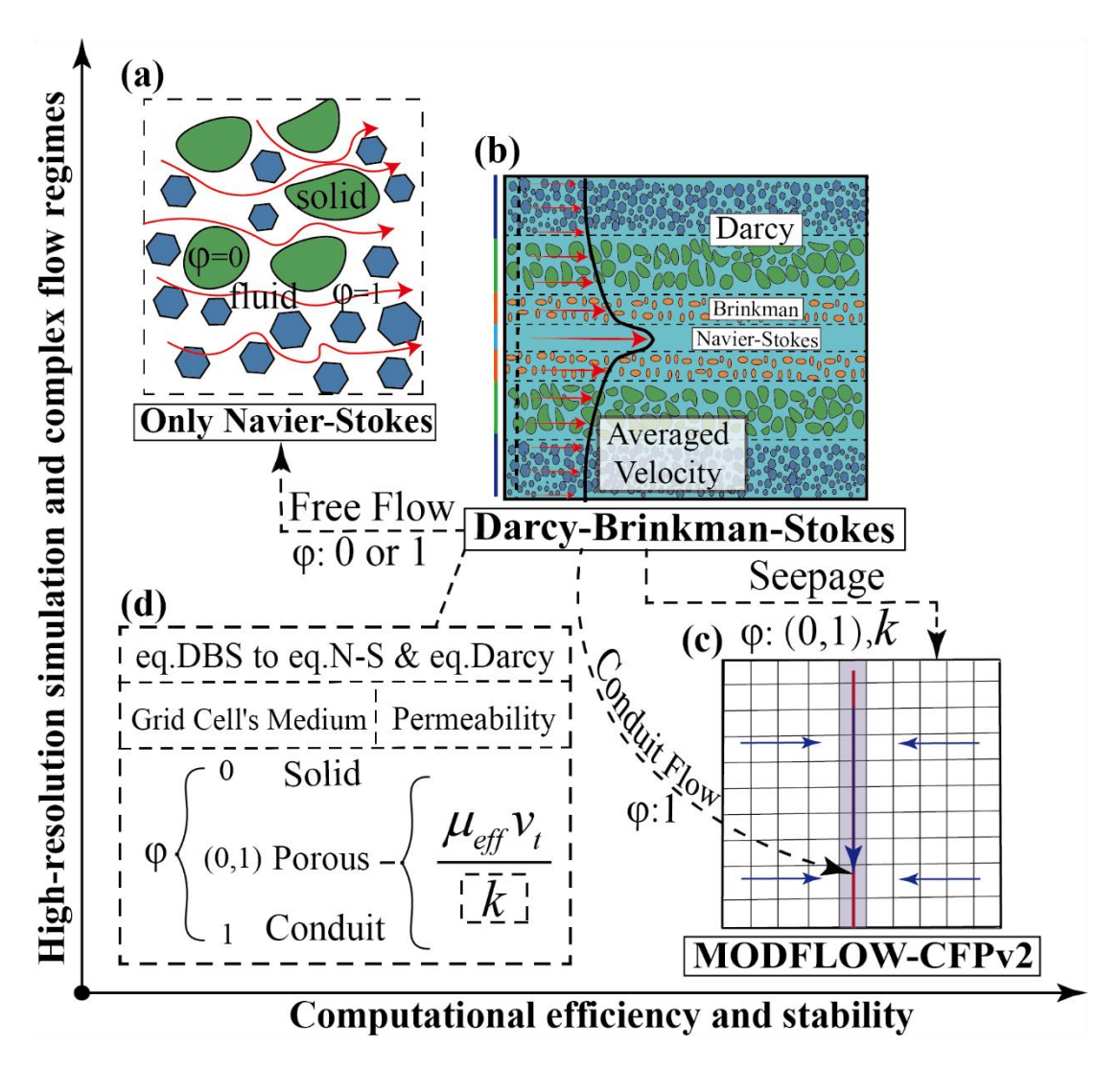


Figure 2. Diagram of performance and applicability of different models, (a) N-S model (Navier-Stokes model), (b) DBS model, (c) Schematic diagram of MODFLOW-CFP model solution, (d) Conversion method from DBS equations to N-S equations and Darcy equations.

(3) Sensitivity and Uncertainty Analysis:

The manuscript currently lacks a detailed sensitivity or uncertainty analysis, which is important to understand how variations in critical parameters (e.g., permeability, porosity, precipitation patterns) might affect the interaction processes described.

We sincerely appreciate your valuable suggestions, which are instrumental in enhancing the quality of our manuscript. The new "4. Uncertainty Analysis" section (lines 693-792) demonstrates that:

(1) Conduit geometry (square cross-sections yield higher peak flows than circular ones)

(2) Permeability of the epikarst zone (higher permeability increases inter-media exchange frequency)

are key factors regulating karst-stream exchanges. This provides prioritization guidance for model parameter calibration.

Lines 693-792:

"4. Uncertainty Analysis and Discussion

The multi-level conduit configuration inherently affects multi-media interactions by simultaneously altering permeability, conduit diameter, and porosity parameters. This study will further conduct sensitivity analyses on individual variables to investigate their impacts on the vulnerability of karst aquifer systems.

4.1 Impacts of Conduit Diameter and Geometry on Interactions Between Karst Aquifer Systems and Streams

Fig. 12 presents hydrographs under conditions of circular conduits with varying radii (r=0.2, 0.3, 0.3, and 0.5 m) and square-section conduits (r=0.5 m) for (a) stream-connected flow, (b) karst spring discharge, (c) epikarst flow, (d) porous medium I (PM I), (e) PM II, and (f) PM III. Fig. 12(c.1) illustrates different conduit cross-sectional shapes to analyze their impacts on the interactive flow between karst aquifer systems and adjacent streams.

As shown in Fig. 12(a), larger conduit radii correspond to higher initial discharge peaks and shorter peak arrival times, indicating enhanced porous medium recharge and faster fluid transmission through larger conduits. Notably, the square-section conduit (s-r_c=0.5) exhibits higher peak discharge than its circular counterpart (rc=0.5) due to its surplus cross-sectional area accommodating greater fluid discharge under identical nominal radii.

Fig. 12(b) demonstrates that karst spring peak discharge increases with conduit radius. At r=0.5 m, the square-section conduit (s-r_c=0.5) achieves higher peak discharge than the circular conduit (r_c=0.5), but displays lower recession flow. This occurs because identical precipitation infiltration recharge leads to greater porous medium storage depletion during peak periods in square conduits, subsequently reducing porous medium-to-conduit recharge during baseflow recession.

Combined analysis of Figs. 12(c), (d), and (e) reveals that conduit radius variations do not significantly affect epikarst hydrographs or PM I/II hydrographs. However, square-section sinkholes modify flow patterns: epikarst hydrographs show lower values under square conduits, while PM I/II hydrographs exhibit higher values due to enhanced epikarst groundwater collection in square cross-sections, increasing recharge to PM I/II.

Fig. 12(e) indicates that larger conduit radii correspond to lower negative values. Combined with Fig. 12(a), this demonstrates that increased stream recharge through larger conduits elevates both stream peak discharge and water levels, thereby enhancing porous medium-stream interactions. Similarly, Fig. 12(f) shows that larger conduit radii increase karst spring discharge and PM III hydrograph elevation through enhanced gravity-driven groundwater recharge.

Conduit geometry (radius and shape) constitutes a critical factor in karst aquifer hydrological modeling. Larger circular conduits accelerate peak discharge arrival and amplify stream-connected flow peaks and karst spring discharge. Square-section conduits outperform circular equivalents in peak discharge capacity under identical nominal radii due to cross-sectional area advantages. Enlarged conduits intensify porous medium-stream interactions and amplify PM III recharge through gravitational effects. Comprehensive consideration of conduit geometry impacts on hydrological elements is essential for improving model accuracy and reliability in simulating karst aquifer-stream interaction processes.

4.2 Influence of Permeability on the Interaction Processes Between Karst Aquifer Systems and Streams

The permeability of the epikarst directly controls the ease of fluid infiltration from the surface into the conduit system. Fig. 13 illustrates the hydrological process curves under different epikarst permeability coefficients ($K_E=10^{-6}$, 10^{-7} , 10^{-8} , 10^{-9} ; when $K_E=10^{-9}$, the permeability matches that of porous media, rendering the epikarst incapable of rapid groundwater leakage) for: (a) stream, (b) karst spring, (c) epikarst, (d) PM I, (e) PM II, and (f) PM III. This aims to reveal how epikarst permeability regulates groundwater flow patterns in complex conduit systems and intermedia interactions.

As shown in Fig. 13(a), under high epikarst permeability ($K_E=10^{-6}$): the discharge curve rises rapidly to a peak of ~4.5 m^3/s followed by a sharp decline. This indicates that high permeability enables rapid groundwater leakage from the epikarst to the stream, causing swift flow increases. Peak stream discharge diminishes with decreasing permeability. High permeability reduces flow resistance, facilitating faster fluid entry into the conduit system and generating sharp discharge peaks, while low permeability increases resistance, resulting in gradual fluid release and broader, lower discharge curves.

Fig. 13(b) demonstrates that epikarst permeability differences from porous media have minimal impact on conduit flow. However, when epikarst permeability equals that of porous media ($K_E=10^{-9}$), the peak discharge at the karst spring decreases while maintaining identical baseflow recession characteristics. Combining Figs. 13(c) and (c.1), higher epikarst permeability enhances lateral discharge to the stream. At $K_E=10^{-9}$, gravitational forces dominate vertical recharge to lower media without lateral discharge.

Fig. 13(d) reveals decreasing discharge from Porous Medium I to the stream with reduced epikarst permeability. Cross-referencing Figs. 13(a) and (e), lower epikarst permeability reduces both stream discharge and water level, limiting recharge to Porous Medium II. Fig. 13(f) shows negligible epikarst permeability influence on Porous Medium III's hydrograph.

Epikarst permeability constitutes a critical factor in hydrological modeling of karst aquifer systems. Highly permeable epikarst produces rapid streamflow peaks followed by sharp declines, reflecting efficient groundwater leakage to the stream. Conversely, low permeability yields diminished peaks and broader discharge curves. While karst spring discharge remains relatively stable when epikarst permeability differs from porous media, proper characterization of epikarst permeability is essential for accurately simulating hydraulic interactions between media,

regulating groundwater flow pathways and velocities. This enhances model reliability in capturing complex flow dynamics within karst conduit-stream systems.

4.3 Influence of Porosity on the Interaction Between Karst Aquifer Systems and Adjacent Streams

Fig. 14 presents the hydrographic process curves under different porosity conditions (φ =0.4, φ =0.3, φ =0.2, φ =0.1) for (a) stream, (b) karst spring, (c) epikarst, (d) PM I, (e) PM II, and (f) PM III. Fig. 14(c.1) illustrates the schematic diagram of groundwater flow under different pore sizes. The study aims to elucidate how porosity regulates fluid flow patterns in complex conduit systems.

As shown in Fig. 14(a), lower porosity results in higher flow peaks and earlier peak times. This occurs because reduced pore space limits groundwater storage capacity, forcing excess water to discharge rapidly and elevating the stream hydrograph. Fig. 14(b) demonstrates that lower porosity drives groundwater to preferentially flow through karst conduits and discharge at springs. In Fig. 14(c), the peak discharge of epikarst at $\varphi = 0.4$ slightly exceeds those at $\varphi = 0.3$, $\varphi = 0.2$, and $\varphi = 0.1$.

Fig. 14(d) reveals that at φ =0.1, the storage capacity of porous medium I reaches critical limits. Groundwater recharged from epikarst to porous medium I is rapidly discharged, resulting in significantly higher discharge rates compared to φ =0.3, φ =0.2, and φ =0.1. Fig. 14(e) indicates increased discharge from porous media to the stream as porosity decreases. Combined with Fig. 14(a), reduced porosity enhances stream stage and discharge but diminishes the stream's ability to recharge porous media due to limited storage capacity. Fig. 14(f) shows negligible porosity effects on the hydrograph of porous medium III, as its behavior is primarily governed by conduit flow.

In hydrological modeling, porosity parameters must be calibrated to accurately simulate groundwater flow paths and storage-release dynamics. For low-porosity regions, models should emphasize rapid drainage capacity of conduit systems and transient flow variations. In high-porosity areas, considerations should include fluid retention risks, stream-porous media interactions, and their long-term impacts on geological stability and water resource allocation. Proper porosity parameterization enhances simulation accuracy for diverse hydrological processes, enabling improved prediction and management of karst water resources.

Karst hydrological vulnerability manifests prominently through rapid infiltration, epikarst runoff, groundwater table fluctuations, and abrupt spring discharge variations. The DBS model effectively simulates multi-media interactions during extreme recharge events, enabling temporal analysis of media-stream exchanges, identification of peak interaction values, and applications in coupled conduit flow-seepage processes for two-phase flow systems."

Lines 1074-1101:

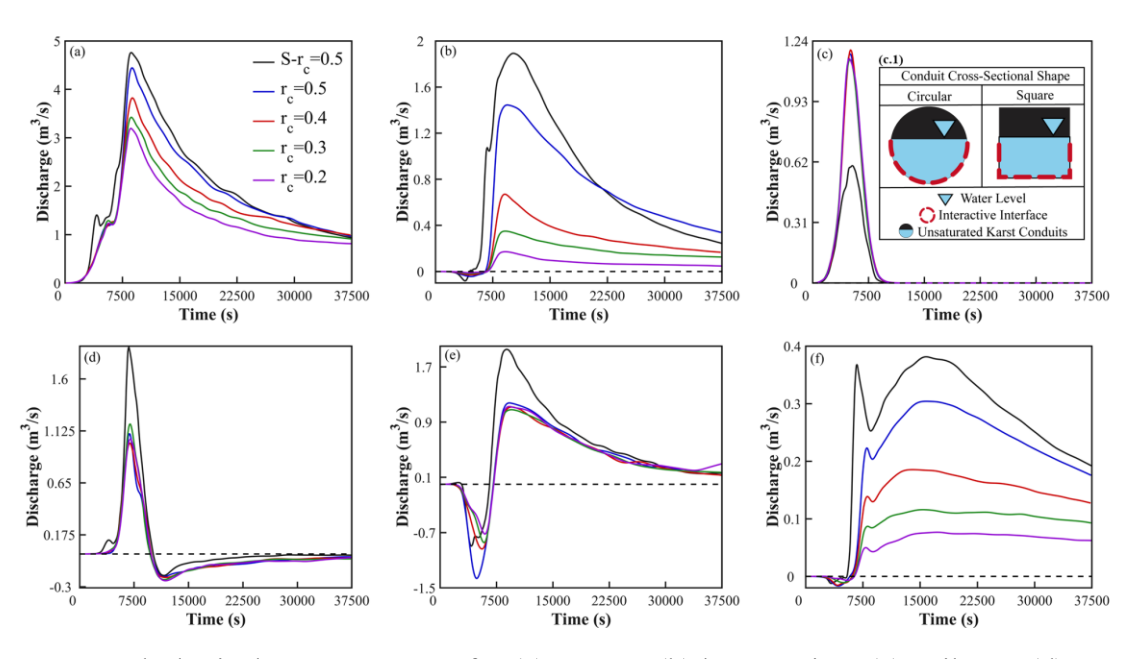


Figure 12. Hydrological process curves for (a) stream, (b) karst spring, (c) epikarst, (d) PM I, (e) PM II, and (f) PM III under conditions of circular conduits with radii $r_c = 0.2, 0.3, 0.3,$ and 0.5, and square-cross-section conduits with S- $r_c = 0.5$. Subplot (c.1) shows a schematic diagram of different conduit cross-sectional shapes.

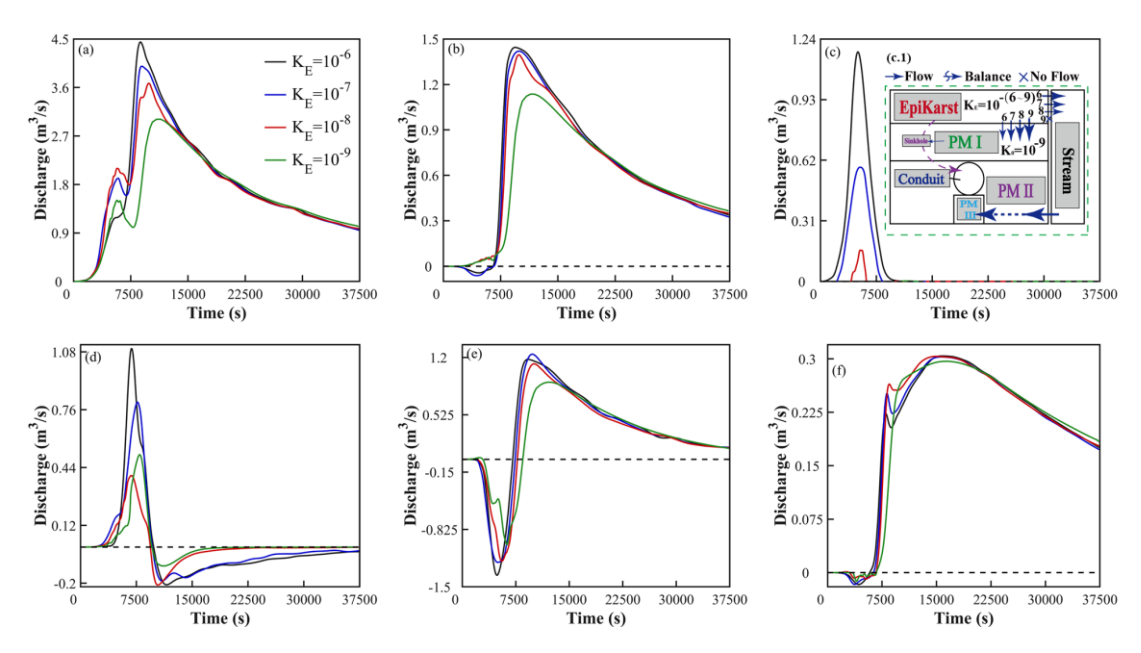


Figure 13. Hydrographs under different epikarst permeability conditions ($K_E=10^{-6}$, $K_E=10^{-7}$, $K_E=10^{-8}$, $K_E=10^{-9}$) for: (a) stream, (b) karst spring, (c) epikarst, (d) PM I, (e) PM II, (f) PM III. Subfigure (c.1) shows a schematic diagram of media interactions under varying epikarst

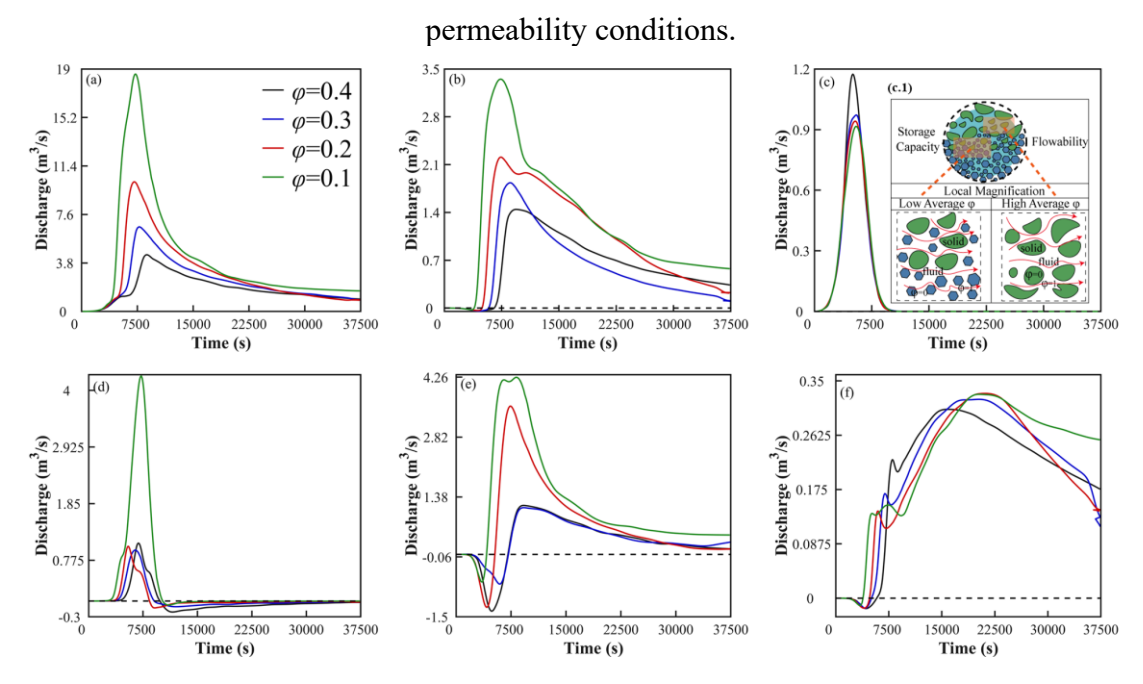


Figure 14. hydrograph curves under different porosity conditions (ϕ = 0.4, ϕ = 0.3, ϕ = 0.2, ϕ = 0.1) for (a) stream, (b) karst spring, (c) epikarst, (d) PM I, (e) PM II, and (f) PM III. Among these, (c.1) illustrates a schematic diagram of the medium's water storage capacity and flow capacity under varying porosity conditions.

(4) The modeling approach is theoretical and numerical. Adding validation using real-world or field observation data could greatly strengthen confidence in the model's predictive capability and practical applicability.

We sincerely appreciate your valuable suggestions, which are crucial for enhancing the quality of our manuscript.

Given the technical challenges in in-situ monitoring of multi-media exchange fluxes, we validated the DBS model's capabilities in variably saturated flow modeling using classical experimental cases (Warrick et al., 1985; Vauclin et al., 1979) (lines 614-633). We are currently collaborating with karst field sites to obtain observational field data.

Lines 614-633:

"The external recharge of the system significantly influences the interaction processes among different media. This study further investigates how the inherent hydrogeological properties of karst systems affect these interactive processes. Variable saturated flow in the karst vadose zone plays a critical role (Dvory et al., 2018), where the water retention characteristics of porous media govern unsaturated flow dynamics. However, the CFPv2 model struggles to simulate variable saturation processes. This paper compares the DBS model results with two distinct experimental datasets to elucidate the advantages and limitations of the DBS approach in simulating variable saturated flow.

Case 1: A typical unsaturated-unsteady seepage problem in sandy clay loam (Warrick et al., 1985), where the soil hydraulic properties are provided by the international UNSODA database (Leij et al., 1996). Key parameters include: $k = 1 \times 10-6$ m/s, $\alpha_s = 0.363$, $\alpha_r = 0.186$, and n = 1.53. The model consists of a vertical soil column (1 m thickness) with an initial pressure head of -8 m across the domain. The top boundary is set to a pressure head of 0 m to simulate free surface infiltration.

Case 2: A 2D laboratory infiltration experiment by Vauclin et al. (1979), widely used for evaluating saturated-unsaturated unsteady seepage models. The soil slab measures 2.00 m in height, 6.00 m in width, and 0.05 m in thickness, with an impermeable base and free drainage boundaries on both sides. Initially, the water table is set at 0.65 m. A central 1.00 m section of the top boundary receives uniform precipitation at 0.148 m/h for 8 hours, during which free surface evolution is monitored. Soil hydraulic properties are described using the van Genuchten-Mualem model with parameters: $k = 0.35 \, m/h$, $\alpha_s = 0.30$, $\alpha_r = 0.01$. Due to symmetry, the DBS model simulates the right half of the domain."

(5) The authors mention fine grid discretization and the Courant number limitations causing small time steps, which implies significant computational costs. A brief discussion of the computational resources required and possible strategies for optimization could enhance the practicality and usability of their approach.

We sincerely appreciate your valuable suggestions, which are crucial for enhancing the quality of our manuscript. The DBS model computations in this study were performed on a Lenovo ThinkSystem SR665 computational server, with optimization strategies relying on domain decomposition-based parallelization.

Lines 301-303:

"However, the DBS model operates in three dimensions (3D), requiring grid refinement around conduits and their vicinity to ensure accurate flow resolution. This increases computational load compared to the 1D conduit flow framework of CFPv2. To address this challenge, all simulations in this study were executed on a Lenovo ThinkSystem SR665 server, which provides the necessary computational power for handling complex 3D meshes."

(6) While the comparison with MODFLOW-CFP is insightful, the manuscript could benefit from clearly highlighting specific scenarios or conditions under which the presented model notably outperforms or underperforms compared to MODFLOW-CFP.

We sincerely appreciate your valuable suggestions, which are crucial for enhancing the quality of our manuscript. We conducted a comparative analysis of the DBS model and CFPv2 model performance.

Lines 293-300:

"2.4.1 DBS Model Conversion and Applicability Assessment

As illustrated in Figure 2, the Navier-Stokes (N-S) model can resolve fine-scale pore-scale flows and perform high-fidelity simulations. In contrast, the CFPv2 model achieves high computational efficiency and stability by discretizing one-dimensional conduits within porous media. The DBS (Dual-domain Brinkman-Stokes) model combines the advantages of both approaches: By incorporating additional resistance source terms into the N-S equations, it maintains high-fidelity flow resolution in conduits. For porous media, it adopts a Darcy-type flow formulation, significantly reducing computational costs."

Lines 1036-1040:

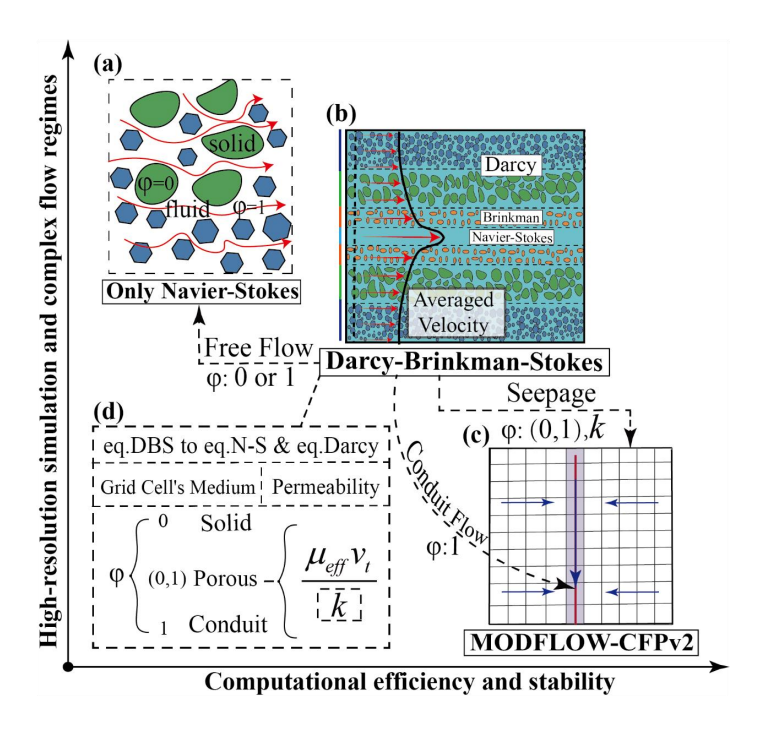


Figure 2. Diagram of performance and applicability of different models, (a) N-S model (Navier-Stokes model), (b) DBS model, (c) Schematic diagram of MODFLOW-CFP model solution, (d) Conversion method from DBS equations to N-S equations and Darcy equations.

(7) I highly recomment to expand your literature review to the integrated models such as SWAT-MODLOW, which are important aspect of your work, I recommend you to cite below papers. Hydrogeological modelling of a coastal karst aquifer using an integrated SWAT-MODFLOW approach ---- Estimating exploitable groundwater for agricultural use under environmental flow constraints using an integrated SWAT-MODFLOW model --- Can Large Language Models Effectively Reason about Adverse Weather Conditions?

We sincerely appreciate your valuable suggestions, which are crucial for enhancing the quality of our manuscript. In the Introduction (Lines 72-76), we have added a discussion on integrated

modeling approaches (e.g., SWAT-MODFLOW), citing your recommended references (Fiorese et al., 2025; Yifru et al., 2024).

Lines 72-76:

"Moreover, this methodology has been extensively applied worldwide for estimating karst groundwater flow and water resources (Chang et al., 2015; Qiu et al., 2019; Kavousi et al., 2020; Gao et al., 2020, 2024), as well as in integrated modeling studies coupling SWAT with MODFLOW to investigate groundwater-surface water interactions (Fiorese et al., 2025; Yifru et al., 2024)."